Analytica Chimica Acta 1197 (2022) 339520

Contents lists available at ScienceDirect

Analytica Chimica Acta

journal homepage: www.elsevier.com/locate/aca

Nitrogen and sulfur co-doping strategy to trigger the peroxidase-like and electrochemical activity of Ti_3C_2 nanosheets for sensitive uric acid detection

Da Chen , Shuaibin Shao , Wei Zhang , Jingbo Zhao , Meiling Lian *

Key Laboratory of Civil Aviation Thermal Hazards Prevention and Emergency Response, Civil Aviation University of China, Tianjin, 300300, PR China

HIGHLIGHTS

- One-step synthesis of nitrogen and sulfur co-doped Ti_3C_2 nanosheets (NS−Ti_3C_2 NSs).
- A new colorimetric and electrochemical coupling sensing platform was established based on NS-Ti_3C_2 NSs for sensing uric acid.
- The developed sensing strategy shows excellent analytical performance.
- Nitrogen and sulfur co-doping is an effective method to improve the peroxidase-like and electrochemical activity of MXene.

GRAPHICAL ABSTRACT

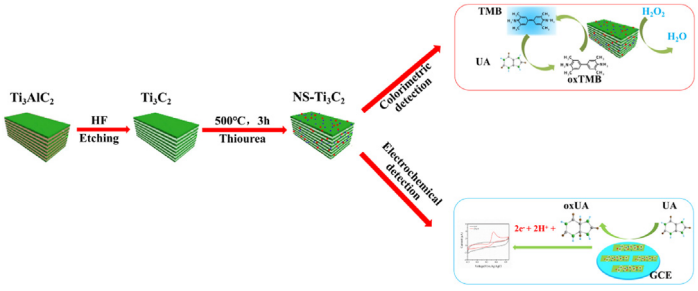

ARTICLE INFO

Article history:
Received 23 September 2021
Received in revised form
20 December 2021
Accepted 17 January 2022
Available online 19 January 2022

Keywords:
Electrochemical
Colorimetric
Biosensor
Uric acid
Ti_3C_2 nanosheets

ABSTRACT

The development of functional nanomaterials based on the unique structure and morphology of MXene for biosensing has aroused great interest. In this work, using thiourea as the doping source, a new structure composed of nitrogen and sulfur co-doped on the surface of Ti_3C_2 nanosheets was synthesized through a simple one-step synthesis method. Fortunately, the obtained nitrogen and sulfur co-doped Ti_3C_2 nanosheets (NS−Ti_3C_2 NSs) showed excellent peroxidase-like activity and electrochemical activity. The catalytic mechanism of modified Ti_3C_2 nanosheets was explored. It is revealed that the catalytic mechanism of NS-Ti_3C_2 NSs is composed of two important parts: the dissociation and adsorption of H_2O_2 and the protonation of TMB. In addition, the fabricated NS-Ti_3C_2 NSs-based electrochemical biosensor is superior to the counterpart from Ti_3C_2 nanosheets, indicating that the doping of nitrogen and sulfur elements provides more active sites and promotes electron transport efficiency. Combining the unique advantages of colorimetry and electrochemical technology, we have developed a fast, accurate, intuitive and efficient UA detection method for uric acid in the range of 2 μM−400 μM with a detection limit (LOD) of 0.19 μM. The established sensing platform in this study prove the possibility of the doping method for the development of MXene-based biosensors with high sensitivity and high performance, and pave the way for the future development of biosensors for biomedical fields.

1. Introduction

MXenes is an emerging two-dimensional conductive material

* Corresponding author.
E-mail address: mllian@cauc.edu.cn (M. Lian).

https://doi.org/10.1016/j.aca.2022.339520
0003-2670/

based on transition metal carbides and nitrides. Since MXene was discovered in 2011, their unique layered structure, abundant surface functional groups, controllable morphology and simple surface modification methods promote their applications in the fields of energy storage and conversion, biometrics and sensing, lighting, purification and separation [1–4]. Especially in the field of biosensors, replacing conventional sensor materials, such as metal alloys and carbon, MXenes is a highly promising alternative sensor material. Many electrochemical, colorimetric or optical biosensors based on MXene have been reported for rapid, simple and label-free detection of biological events [5–7]. Although MXenes has achieved explosive results in biosensing, there are still some challenges to be solved in the future. First of all, the preparation method for MXenes is relatively simple, which results the obtained MXenes only possess relatively single properties and the biosensing performance is unsatisfactory. In order to further improve the performance of MXene-based sensing, researchers have proposed several strategies, including the surface functionalization, the acquisition of single-layer nanosheets, and the formation of composite materials [8–10]. However, the nanosheets will undergo aggregation and pore deformation, resulting in loss of active sites during sensing applications. Besides, Although MXene has been widely used in the field of colorimetry and electrochemistry [11,12], the colorimetric and electrochemical coupling technology based on MXene has been less studied. Therefore, much effort should focus on exploring more colorimetric, electrochemical, and coupling technologies platform, and develop nanoenzymes catalytic system based on MXenes to expand its biological analysis application field.

Specific surface area and catalytic active sites are two important factors to improve catalytic efficiency, many material synthesis methods had been developed to improve these two factors. Among them, Heteroatom-doped carbon materials (HDCM), as a new type of heterogeneous catalyst, have attracted appreciable scientific interest in metal-free catalysis in recent years [13]. Heteroatom-doping provides additional heteroatom-containing active species into the carbon matrix and alters the structural and electronic properties of carbon materials [14], enhancing the catalytic performance of the material. Compared with other methods, nonmetal doping is a more economical and convenient material modification method. As one of the most common doping elements, nitrogen-doped MXene has been widely used in hydrogen evolution reaction (HER) and electrochemical energy storage [15,16]. Some studies found that the introduction of sulfur heteroatoms into the nitrogen-doped shell will enhance the electron transfer process and sulfur doping increases the interlayer spacing at the atomic level, providing more space and active sites [17–19]. Noticeably, doping two types of elements into carbon materials can enhance reaction kinetics, exhibiting superior performance compared with single-doped carbon catalysts [20]. Due to the excellent performance of nitrogen and sulfur in MXene, most scholars' research has focused on electrochemical energy storage, but research on nanozymes and electrochemical detection are still rare. In addition, the unclear catalytic mechanism of MXene as a nanozyme is a major problem that plagues the scientific community. Therefore, it is of great significance to explore the efficient design and catalytic mechanism of MXene in the field of biosensing.

In this study, using thiourea as the doping source, we synthesized NS-Ti_3C_2 NSs via a simple one step for the non-enzymatic colorimetric and electrochemical uric acid (UA) detection (Scheme 1). Interestingly, compared with Ti_3C_2 NSs, NS-Ti_3C_2 NSs not only possessed peroxidase-like activity, but also exhibited excellent electrochemical performance. The peroxidase-like catalytic activity performance of NS-Ti_3C_2 NSs was employed in the presence of H_2O_2-containing peroxidase substrate 3,3′,5,5′-tetramethylbenzidine (TMB). The mechanism for high-efficiency peroxidase-like activity exhibited by NS-Ti_3C_2 NSs was discussed. Furthermore, in order to study the feasibility of electrochemical properties of NS-Ti_3C_2 NSs, it was used to fabricate the sensor for the detection of UA by immobilizing it on a glassy carbon electrode (GCE). Finally, the impact of this appreciated scheme for the UA sensing was successfully investigated.

2. Experimental

2.1. Chemicals

3,3′,5,5′-tetramethylbenzidine (TMB, 99.5%), Dimethyl sulfoxide (DMSO, 99.8%), limonexic acid (99%), disodium phosphate dodecahydrate (99%), tyrosine (99%), urea (99%), copper(II) chloride dihydrate (98%), diammonium 2,2′-azino-bis(3-ethylbenzothiazoline-6-sulfonate) (ABTS, 98%), dextrose (99%), uric acid (98%), isopropanol (IPA, 99%), terephthalic acid (TA, 99%), ascorbic acid (AA, 98%), cysteine (98%) were purchased from Zhengzhou Acme Chemical (China). Potassium chloride, sodium chloride, ethanol were obtained from Tianjin Aiteyefeng Commercial Development Chemical Branch (China). Hydrogen peroxide(H_2O_2, 30%) was purchased from Tianjin Solomon Biological Technology (China). Ti_3AlC_2 nanosheets was purchased from beike 2D materials Co., Ltd(China). Thiourea (99%) was obtained from Shanghai Aladdin Biochemical Technology (China). Goat serum was purchased from Shanghai Biyuntian Biotechnology. All chemicals were of analytical grade and could be used directly without additional purification. Deionized water was utilized throughout the whole experiment.

2.2. Instruments

The structures of the NS-Ti_3C_2 NSs were characterized by an Quanta 250 FEG SEM. The X-ray diffraction (XRD) pattern for the NS-Ti_3C_2 NSs was obtained by the powder X-ray diffractometer with Cu-Kα radiation (Ultima IV). Characterization of the X-ray photoelectron spectra (XPS) was carried out on the Kratos AXIS SUPRA spectrometer. Fluorometric experiments were carried out on a spectrofluorophotometer of Beijing University of Chemical Technology (China). UV–vis spectra were measured from a Shimadzu UV–Vis spectrophotometer (UV-1780). The raman spectrogram was obtained from the raman spectrometer made by the Civil Aviation Safety and Environment Intelligent Monitoring Laboratory of Civil Aviation University of China. Electrochemical experiment data were collected using a electrochemiluminescence system with a three-electrode (LK5100), platinum wire was used as the auxiliary electrode, Ag/AgCl was used as the reference electrode, and the glassy carbon electrode (GCE) (diameter = 3 mm) modified with nanocomposites served as the working electrode.

2.3. Preparation of the nitrogen and sulfur co-doped Ti_3C_2 nanosheets

NS-Ti_3C_2 NSs were prepared by hydrofluoric acid etching strategy and thiourea grinding process. All reagents were of at least analytical grade. First, lithium fluoride (1.6 g) was dissolved in hydrochloric acid (20 mL, 9 M) by stirring for 5 min, then Ti_3AlC_2 (1 g) is slowly added and stirred at 45 °C for 24 h. The mixture was washed through with deionized water, centrifuged for 6–8 times until the supernatant reached pH of 6. Then the precipitate was dissolved in 100 mL deionized water and sonicated for 3 h under the atmosphere of argon. Finally collect the supernatant by centrifugation (3500 rpm, 1h) to obtain the Ti_3C_2 nanosheets.

The second step is the grinding process of thiourea, the main function is to dope nitrogen and sulfur. Firstly, the mixture of Ti_3C_2

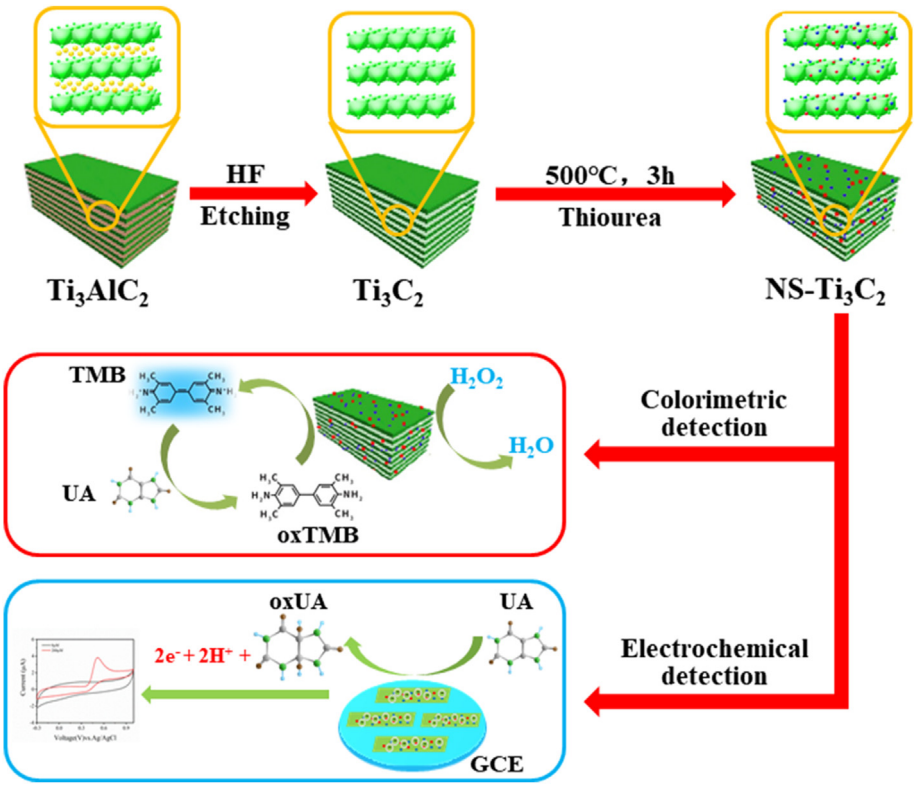

Scheme 1. Schematic illustration of the synthesis and application of NS-Ti_3C_2 NSs.

(100 mg) and thiourea (300 mg) are grinded uniformly, and put it in an argon-filled atmosphere furnace and raise the temperature to 500 °C. After keeping the temperature (500 °C) for 3 h, it is cooled to room temperature along with the furnace. After the product was ground again, it was washed with deionized water until the pH of the supernatant was close to 7. The NS-Ti_3C_2 can be obtained after the final drying process.

2.4. Peroxidase-like activity of nitrogen and sulfur co-doped Ti_3C_2 nanosheets

In order to evaluate the peroxidase-like activity of NS-Ti_3C_2 NSs, the catalytic oxidation reaction of TMB mediated with H_2O_2 was performed. Typically, 100 μL of NS-Ti_3C_2 NSs dispersion solution (4 mg mL^{-1}) was added into the mixture of 1700 μL of disodium hydrogen phosphate-citrate buffer (pH = 4.2), 100 μL of 20 mM TMB (DMSO solution), and 100 μL of 1 M H_2O_2; then, the obtained mixture was shaken and incubated in a water bath (40 °C, 10 min). The formation of the oxidized TMB was recorded by UV−visible spectrophotometer monitoring the absorbance changes at 652 nm after 10 min incubation. In addition, ABTS is also used as substrates for Peroxidase-like mimicking similar with that of TMB. In the experiment for steady state kinetic analysis, the concentrations of TMB and H_2O_2 were changed while the other conditions were fixed, and the absorbance values at 652 nm were immediately recorded after 10 min, obtaining the Michaelis-Menten of NS-Ti_3C_2 NSs curves. The Michaelis-Menten constant (Km) is obtained using Lineweaver-Burk double reciprocal graph: $\frac{1}{v} = \frac{Km}{S \cdot Vmax} + \frac{1}{Vmax}$, where, v = initial velocity, S = substrate concentration and Vmax = maximal reaction velocity. Km is the concentration of substrate at which reaction rate is Vmax/2, which represents the affinity between the substrate and the enzyme.

2.5. Fabrication of the electrochemical sensor

Prior to the modification, GCE was polished with 0.05 μm alumina slurry, then the electrode was ultrasonically cleaned in deionized water for 2 min and dried at room temperature. 7 μl of NS-Ti_3C_2 NSs solution (2 mg/mL) was dropped on the cleaned electrode, and after drying in the air overnight, it was used as a working electrode for UA detection. Cyclic voltammetry (CV) responses with the range of −0.3–1.0 V were recorded at disodium hydrogen phosphate-citrate electrolyte (pH = 5.2).

2.6. Detection of UA

As UA can reduce the oxidation state of TMB(blue) to TMB(colorless), the concentration of UA can be detected by monitoring the absorbance changes before and after the UA enters the system. First, 100 μL of NS-Ti_3C_2 NSs dispersion solution (4 mg mL^{-1}), 1700 μL of disodium hydrogen phosphate-citrate buffer (pH = 4.2), 100 μL of 20 mM TMB, 100 μL of 200 mM H_2O_2 were mixed. Then 100 μL of UA solution with different concentrations were added separately, the reaction system were shaken and incubated in a water bath (40 °C, 10 min). Finally, the mixed solution was monitored using a UV−visible spectrophotometer directly at 652 nm.

To carry out the selectivity of NS-Ti_3C_2 NSs in UA detection, in control experiments, 100 μL of potential interfering substances, including ascorbic acid(AA) (4 mM), cysteine(Cys) (4 mM), Cu^{2+} (200 mM), Na^{+} (200 mM), K^{+} (200 mM), tyrosine(Tyr) (200 mM), as well as urea (200 mM) and glucose(Glu) (200 mM), were added instead of UA (4 mM). As for various potential interfering substances coexisting in real samples, the anti-interference ability of the sensing platform is proved by monitoring the absorbance (652 nm) in the copresence of UA and interfering substances. All experiments were performed under optimal conditions. For UA

determination in serum, the samples (obtained from Beyotime, Shanghai, China) were first dealed with centrifugation (4000 rpm, 5 min) to eliminate the protein species, and then the supernatants were collected and diluted (20-fold) with disodium hydrogen phosphate-citrate buffer (pH = 8) for the next-step assay as mentioned above.

When using electrochemical workstation to detect UA, 25 μL of UA solution (20 mM) was added to 5 mL of electrolyte, and then the change in current value is observed by cyclic voltammetry. The volume and concentration of interfering substances used in selective experiments were the same as above, and the preparation of the serum sample is the same as the colorimetric detection procedure.

3. Results and discussion

3.1. Characterization of nitrogen and sulfur co-doped Ti_3C_2 nanosheets

NS-Ti_3C_2 NSs were synthesized by a one-step procedure. First, Ti_3C_2 NSs MXene was synthesized by etching out the intermediate layer from ternary-layered carbide of the MAX phase. Then, using thiourea as the source of heteroatoms, NS-Ti_3C_2 NSs were successfully synthesized by a simple method. As shown in the scanning electron microscope (SEM) image, Ti_3C_2 NSs exhibit microscale bulk sheets with graphene-like multilayer nanostructure (Fig. 1(a)). It was conspicuous that the NS-Ti_3C_2 NSs maintained the multilayered morphology and the open channels of Ti_3C_2 NSs. According to the Energy dispersive X-ray spectroscopy (EDS) spectra of NS-Ti_3C_2 NSs and Ti_3C_2 NSs (Fig. S1), the content of Ti and F decreased significantly after N and S doping. The possible reason was that high temperature makes it easier for N and S to anchor on Ti and F defects [21,22]. More interestingly, the doping of N and S elements further reduced the content of Al element. This may be related to the expansion of the interlayer spacing due to the doping of N and S elements, which made the Al element remaining in MXene easier to fall off. EDS mapping (Fig. 1(c)) confirmed that the presence of nitrogen, sulfur, carbon and titanium in the NS-Ti_3C_2 NSs, and each element was evenly distributed on the surface. The XRD was used to further prove the synthesis of NS-Ti_3C_2 NSs and Ti_3C_2 NSs. As shown in Fig. 1(d), the (002) peak of Ti_3C_2 shifted to a lower angle, indicating that the interlayer spacing became larger [6,10,23,24]. The (104) peak intensity decreased sharply, indicating the formation of Ti_3C_2 [23]. The D peak at about 1350 cm^{-1} in the raman spectrum indicates the inherent defects of the carbon material, while the G peak at about 1580 cm^{-1} reflects the degree of graphitization of the carbon material [25]. The higher the ratio (ie, I_D/I_G), the more defects in the material. The raman spectra of NS-Ti_3C_2 NSs and Ti_3C_2 NSs (NS—Ti_3C_2 NSs I_D/I_G = 0.95, Ti_3C_2 NSs I_D/I_G = 0.92) indicated that the doping of N and S elements made Ti_3C_2 NSs defects had greatly increased (Fig. S2(a)), which also proved SEM image and EDS spectra defect formation conclusion.

To further investigate the compositions and electronic states of the synthesized NS-Ti_3C_2 NSs, XPS characterization was conducted. As shown in Fig. 2(a), C 1s, Ti 1s, N 1s and S 2p peaks were shown in the survey spectrum. The C 1s region was deconvoluted into four components in Fig. 2(b). 284.5 eV, and 288.8 eV are corresponding to the C—C/C═C, and O—C═O [26]. Interestingly, a strong C—S—C an C—N—C bond at 284.9 eV and 286.0 eV can be deconvoluted in the XPS spectrum of NS-Ti_3C_2 NSs, indicating that N and S has been doped in NS-Ti_3C_2 NSs [27]. Fig. 2(c) shown the N 1s fine spectrum, in which the peaks were assigned to the pyridinic-N (398.2 eV), pyrrolic-N (399.6 eV), graphitic-N (401.5 eV) and oxidized-N (402.4 eV) [28,29]. Liu et al. found that the peak of pyrrolic-N is 400.0eV in the N 1s fine spectrum of N—Ti_3C_2 NSs [30], this peak was about 0.4 eV higher than the binding energy of pyrrolic-N of

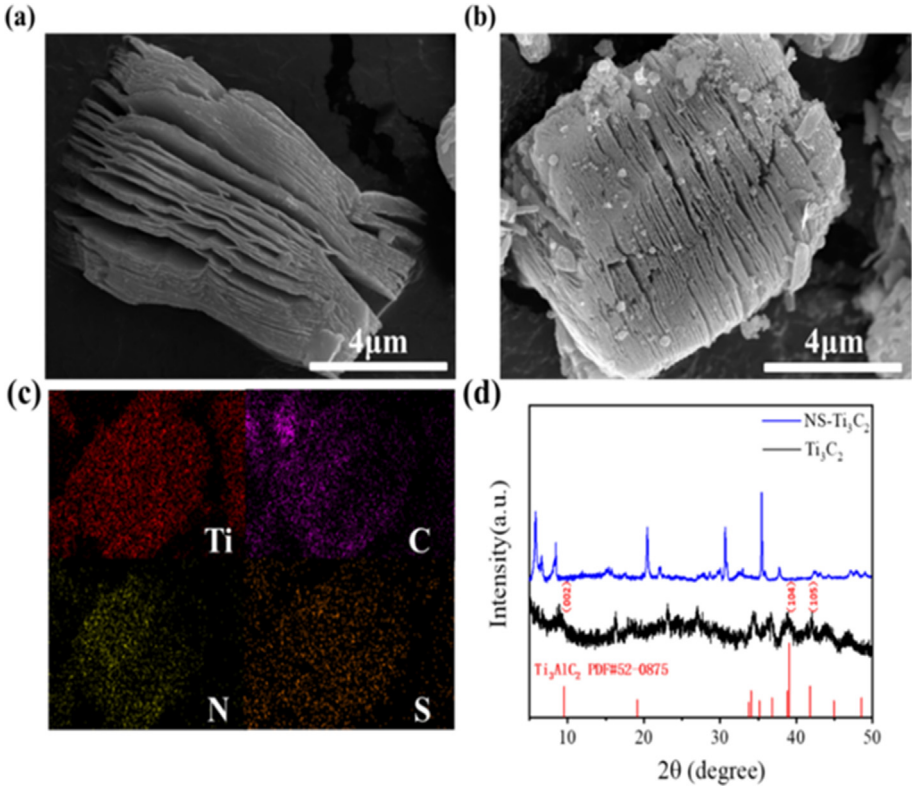

Fig. 1. SEM images for (a) Ti_3C_2 NSs, (b) NS-Ti_3C_2 NSs. (c) EDS elemental mapping of Ti, C, N and S in NS-Ti_3C_2 NSs. (d) XRD pattern of the obtained NS-Ti_3C_2 NSs and Ti_3C_2 NSs.

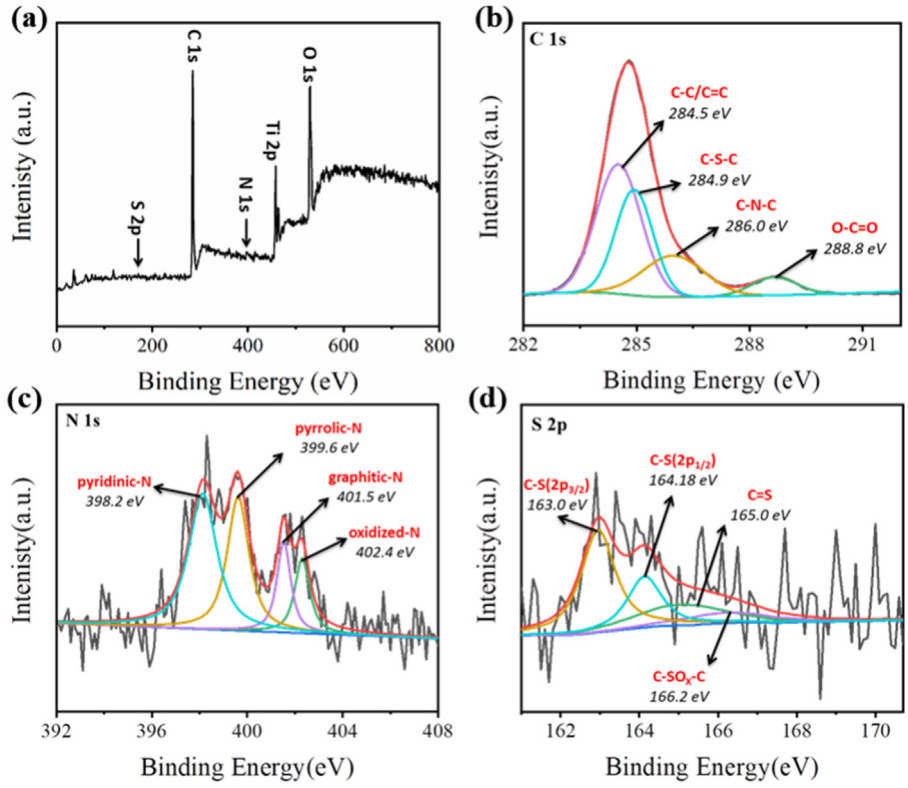

Fig. 2. XPS spectra of the obtained NS-Ti_3C_2 NSs: (a) full survey spectrum, (b) C 1s, (c) N 1s, (d) S 2p.

NS-Ti_3C_2 NSs. This phenomenon indicated that compared with the more electronegative nitrogen, the introduction of sulfur increases the outer valence electron density and weakens the attractive force of the nucleus, resulting in a decrease in binding energy. The spectrum of S 2p displayed four characteristic peaks indexed to C—S($2p_{3/2}$), C—S($2p_{1/2}$), C═S, and C-SO_X-C (Fig. 2(d)), two peaks at 163.0 eV and 164.18 eV could be assigned to the S $2p_{3/2}$ and S $2p_{1/2}$ peaks, indicating that sulfur has been doped in NS-Ti_3C_2 NSs to form the C—S—C covalent bond [26,31]. For Ti 2p XPS spectra, there was no existence of Ti—S species in Ti 2p, possibly because that Ti atoms tended to be replaced by S atoms or N atoms (Fig. S2(b)).

3.2. Peroxidase-like activity of nitrogen and sulfur co-doped Ti_3C_2 nanosheets sensing

To evaluate whether the NS-Ti_3C_2 NSs possess peroxidase-like activities, two well-established probe reaction in the presence of H_2O_2 were selected, the oxidation of TMB and ABTS. The colored oxidation products of TMB and ABTS were known to have maximum absorption peaks at 652 nm and 415 nm, respectively. As shown in Fig. 3(a and b), the color of the reaction system didn't change until adding both H_2O_2 and NS-Ti_3C_2 NSs. These results further confirmed that presence of both H_2O_2 and NS-Ti_3C_2 NSs was required for the oxidation of TMB as well as ABTS. Therefore NS-Ti_3C_2 NSs could be employed as excellent peroxidase mimics.

The optimal parameters of NS-Ti_3C_2 NSs as peroxidase-like enzymes were determined by adjusting the external and internal conditions such as reaction time, temperature, pH, TMB concentration, H_2O_2 concentration and catalyst concentration. The reaction time optimization experiment is shown in Fig. S3(a), the spectrum and inset showed that the absorbance of the reaction system slowed down after 10 min, so 10 min was taken as the optimal reaction time. Temperature experiment displayed that 40 °C can be used as the best reaction temperature (Fig. S3(b)). In addition, Figs. S3(c—f) studied the effects of different pH, NS-Ti_3C_2 NSs, TMB concentration and H_2O_2 concentration on the reaction system. It was determined that the pH was 4.2, the concentration of TMB was 1 mM, the concentration of H_2O_2 was 50 mM, and the concentration of NS-Ti_3C_2 NSs was 0.2 mg/mL as the best conditions for enzyme activity. To analyze the reproducibility of the NS-Ti_3C_2 NSs as peroxidase-like enzymes, under the optimal conditions, the relative enzyme activity of the repetitive experiments was all above 90% (Fig. S4(a)). In addition, NS-Ti_3C_2 NSs still had excellent peroxidase activity after being stored at room temperature for one month (Fig. S4(b)). These results showed that the NS-Ti_3C_2 NSs has reproducible and long-term stable peroxidase activity.

In order to better evaluate the peroxidase-like activity of NS-Ti_3C_2 NSs, steady-state kinetic analysis was performed on them under optimal conditions. Using TMB and H_2O_2 as substrates, a series of experiments were carried out by changing one of the substrates while keeping the other substrate unchanged (Fig. 3(c and d)). When the concentration of H_2O_2 remained unchanged and the concentration of TMB was changed, the calculated K_m of NS-Ti_3C_2 NSs with the substrate of TMB is 0.13 mM, which is lower than the value of MXene@NiFe-LDH [32], HRP [33], Cu NCs [34], CeO_2 NPs [35], indicating that NS-Ti_3C_2 NSs have a much better affinity than HRP with TMB as the substrate. When the concentration of TMB remained unchanged and the concentration of H_2O_2 was changed, the K_m value with the substrate of H_2O_2 is 5.46 mM, indicating that the good affinity of NS-Ti_3C_2 NSs and H_2O_2. The detailed steady-state kinetic values for TMB and H_2O_2 was given in Table S1.

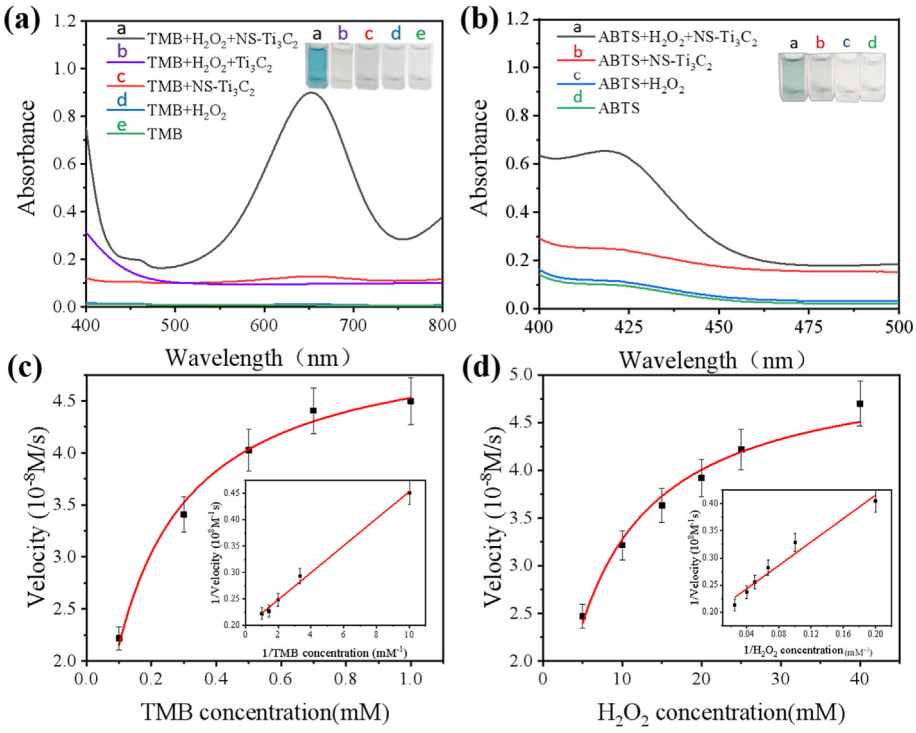

Fig. 3. UV−visible absorption spectrum of (a) TMB and (b) ABTS in different reaction systems, inset: corresponding color change. Steady-state kinetic assay of NS-Ti_3C_2 NSs by varying the TMB concentration at a fixed concentration of H_2O_2 (c) and varying H_2O_2 concentration at a fixed concentration of TMB (d), the inset shows the corresponding Lineweaver-Burk plots of the double reciprocal of Michaelis Menten equation. (For interpretation of the references to color in this figure legend, the reader is referred to the Web version of this article.)

3.3. *Catalytic mechanism of nitrogen and sulfur co-doped Ti_3C_2 nanosheets*

The determination of the type of catalytic reaction is the prerequisite for studying the reaction mechanism. Normally, the peroxidase mechanism does not produce gas [36], but recent studies had found that Fe_3O_4@SiO_2−NH_2−Au@PdNPs could act as a peroxidase to cause the color reaction of TMB with oxygen generation [37]. Fig. S5 revealed the change of the state of the reaction system with time under the optimal conditions, which was used to prove whether there was gas generation. The colorless solution was the control group (without TMB), which was used to eliminate the influence of the gas generated by the self-decomposition of hydrogen peroxide. No bubbles were observed on the test tube wall within 20 min, which proved that the reaction system did not generate gas [38], so products of the reaction were H_2O and oxTMB.

According to reports, the catalytic mechanism of the nanocatalyst is a Fenton-like catalytic reaction generating •OH due to the decomposition of H_2O_2 [39]. Density functional theory had been used to reveal the dissociation and adsorption of H_2O_2 in peroxidase-like enzymes [40]. In addition, the adsorption performance of MXene is related to the type and number of functional groups on the surface. Feng et al. found that MXene synthesized by high-frequency etching has a large number of −F functional groups, and this functional group is not conducive to the improvement of adsorption performance [41]. The EDS spectra of two materials (Fig. S1) shown that nitrogen and sulfur doping greatly reduces −F functional groups, which created favorable conditions for the improvement of the adsorption performance of the material. Based on the existing reports, the catalytic mechanism can be divided into two parts: the dissociation and adsorption of hydrogen peroxide and the protonation of TMB (Fig. 4). •OH and protonated TMB undergo a violent electron transfer on the surface of NS-Ti_3C_2 NSs to generate oxidation states TMB (oxTMB) and H_2O.

The decomposition and adsorption of H_2O_2 were the basis of the reaction. In an aqueous solution without metal ions, the dissociation energy of the O−O bond in H_2O_2 is close to the energy released by the decomposition of H_2O_2 [42], which provides the possibility for the decomposition of H_2O_2 into •OH. In addition, for nitrogen-doped carbon materials, the lone pair of electrons in pyridine N can induce the adsorption of •OH on its surface, endowing them with the hydrophilicity and adsorption capability towards positive charged molecules [43]. The presence of sulfur can change the spin and charge density of the catalyst and further improve the catalyst activity [44]. After TA captures •OH, the product will emit strong fluorescence at 435 nm. Using this phenomenon proved the generation of •OH (Fig. 5(a)). When there was only TA in the reaction system, the fluorescence intensity couldn't be detected. When H_2O_2 and Ti_3C_2 NSs were added, the fluorescence intensity had an upward trend, indicating that a very small part of H_2O_2 was decomposed into •OH. When H_2O_2 and NS-Ti_3C_2 NSs were added, the fluorescence intensity rose rapidly, indicating that a large amount of •OH was produced. The IPA scavenging experiment further proved the production of •OH in the reaction system (Fig. 5(b)). When the scavenger (IPA) was added, the absorbance value of the reaction system became 1/3 of the original, indicating that H_2O_2 could be Catalyzed by NS-Ti_3C_2 NSs to produce a large amount of •OH.

The redox of TMB and H_2O_2 is an electron transfer process. The electrocatalytic behavior of Ti_3C_2 NSs and NS-Ti_3C_2 NSs modified glassy carbon electrode (GCE) toward the electrochemical redox of TMB and H_2O_2 was studied using cyclic voltammetry (CV). It is found that two pairs of redox peaks of TMB in the modified GCE, and the oxidation potentials of NS-Ti_3C_2 NSs/GCE are negatively shifted and the peak currents increase as compared to Ti_3C_2 NSs/GCE (Fig. 5(c)) [45]. In addition, it can be seen from Fig. 5(d) that the

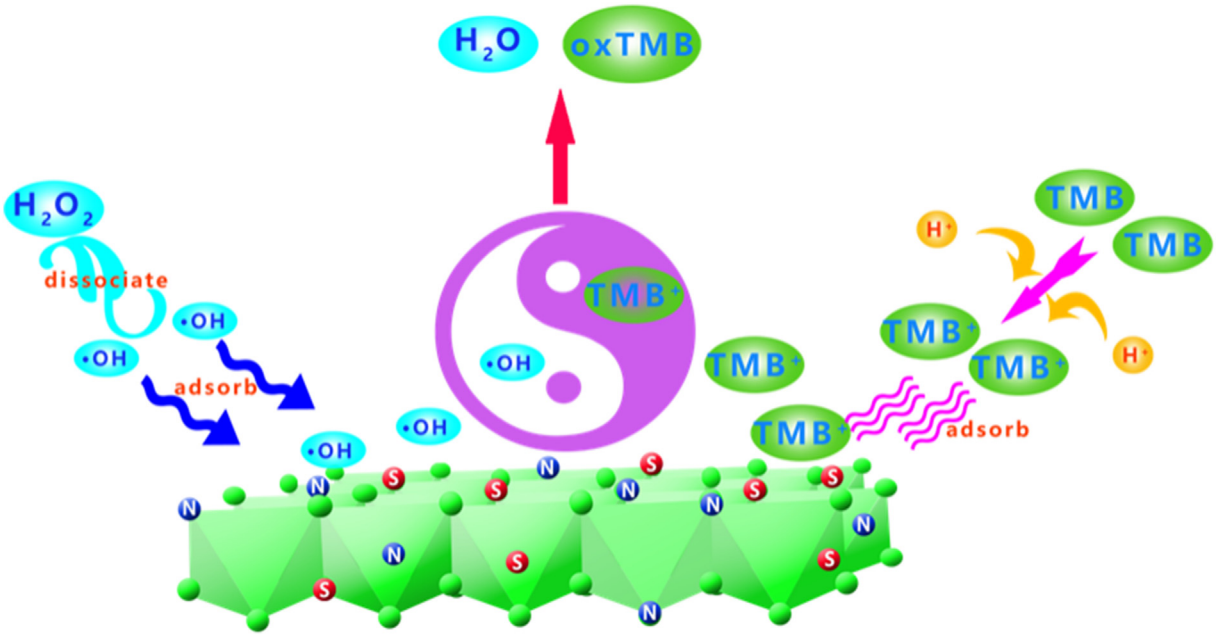

Fig. 4. Mechanism of the NS-Ti_3C_2 NSs in the reaction system.

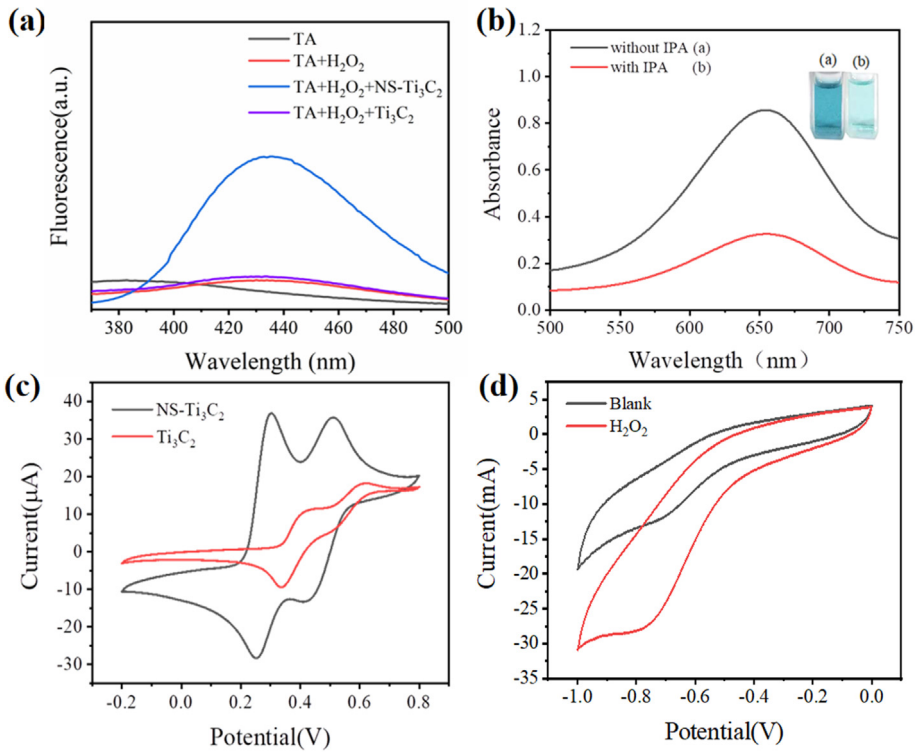

Fig. 5. (a) Fluorescent spectra of the different reaction systems. (b) Absorbance spectra of ox-TMB in the presence of hydroxyl radical scavenger (IPA) in the reaction system of TMB + H_2O_2+NS-Ti_3C_2 NSs, inset: corresponding color change. (c) CV of Ti_3C_2 NSs/GCE and NS-Ti_3C_2/GCE in the presence of TMB in disodium hydrogen phosphate-citrate buffer (pH = 5.2) with the scan rate of 100 mV s^{-1}. (d) CV of NS-Ti_3C_2/GCE with and without H_2O_2 in disodium hydrogen phosphate-citrate buffer (pH = 5.2) with the scan rate of 100 mV s^{-1}. (For interpretation of the references to color in this figure legend, the reader is referred to the Web version of this article.)

current increased significantly for the NS-Ti_3C_2 NSs-modified GCE to H_2O_2 compared to Ti_3C_2 NSs/GCE. These results indicate that the Ti_3C_2 NSs doped with nitrogen atoms can exhibit electrocatalytic activity for TMB and H_2O_2, and significantly accelerate the electron transfer [46].

3.4. Electrochemical activity of nitrogen and sulfur co-doped Ti_3C_2 nanosheets

As the typical substrate material, Ti_3C_2 NSs had been widely used in the study of electrochemical sensors, so we studied the

electrochemical behavior of Ti_3C_2 NSs and NS-Ti_3C_2 NSs for UA by cyclic voltammetry (CV). As shown in Fig. 6(a), a well-defined oxidation peak and a broad reduction peak appeared on NS-Ti_3C_2/GCE, which is due to the fact that UA is first oxidized to quinonoid and then undergoes a rapid chemical reaction [47]. In addition, the sensitivity of an electrochemical sensor is significantly affected by the pH value and the volume of the electrochemical substrate solution (NS−Ti_3C_2 NSs). We determined the optimal pH value (pH = 5.2) and the volume of the NS-Ti_3C_2 NSs (7 μL) by optimizing the parameters (Fig. 6(b and c)). In addition, we found that there was a good linear relationship between the square root of the scan rate and the current intensity (Fig. 6(d)), the linear regression equation is: $I_p = -1.125 + 0.471\ V^{1/2}$, $R^2 = 0.995$, indicating that the electrochemical reaction of UA catalyzed by NS-Ti_3C_2 NSs/GCE is a typical diffusion control process [48]. As a result, the diffusion controlled electron transfer for NS-Ti_3C_2/GCE allowed the detection of UA (Scheme 1).

3.5. Detection of UA

UA, as a product of the supersession of purine nucleotides, is an important biomarker for many diseases [49,50]. High uric acid concentration can cause hyperuricemia which is closely related to gout, arthritis, kidney disease, and cardiovascular disease [51,52]. Therefore, monitoring uric acid is of great significance for early diagnosis of diseases related to their activities [53]. Colorimetry has received widespread attention due to its rapidity, simplicity and visualization [54]. For instance, Zheng et al. designed a colorimetric method for the determination of UA with use of a smartphone [55]. However, the colorimetric method has the disadvantage of poor selectivity. Therefore, it is necessary to design more sensitive and selective strategies to meet the detection requirements. Electrochemical technology has achieved higher sensitivity and selectivity in real-time analysis, which can detect a variety of analytes at different potentials [56,57]. Based on the excellent POD and electrochemical activity of NS-Ti_3C_2 NSs, we designed a strategy to complement these two technologies for the detection of UA.

First of all, a new uricase-free biosensor has been obtained for UA colorimetric sensing. This device is based on the inhibition of the TMB color reaction by UA (Scheme 1). Fig. 7(a) showed the UV−vis absorption spectra measured with adding different concentrations of UA. Obviously, the absorption peak decreased gradually along with the increase of UA concentration. Moreover, the blue color faded to colorless, which could be visualized easily through eyes. The good dose response of the absorbance upon the UA concentration in the range of 5−400 μM, and the detection limit was found 1 μM (Fig. 7(b)). Therefore, the sensor system could meet the daily uric acid detection requirements.

Furthermore, we explored the application of NS-Ti_3C_2 NSs as catalytic sensing materials for UA monitoring in electrochemical sensing. With optimized parameters as experimental conditions, disodium hydrogen phosphate-citrate buffer (pH = 5.2) was used as the electrolyte, the CV responses of the NS-Ti_3C_2 NSs/GCE with different concentrations of UA were measured (Fig. 7(c)). With the increase of UA concentration, the peak current density increases linearly (Fig. 7(d)). In the UA concentration range of 2 μM−34 μM, the linear equation is: $j_1 = 0.242 + 0.334C_{UA}$, $R^2_{j1} = 0.995$. In the UA concentration range of 34 μM−280 μM, the linear equation is: $j_2 = 6.529 + 0.137C_{UA}$, $R^2_{j2} = 0.992$. The detection limit was 0.19 μM, indicating that the electrochemical method has higher sensitivity than the colorimetric.

Table S2 summarized the UA detection methods used in this

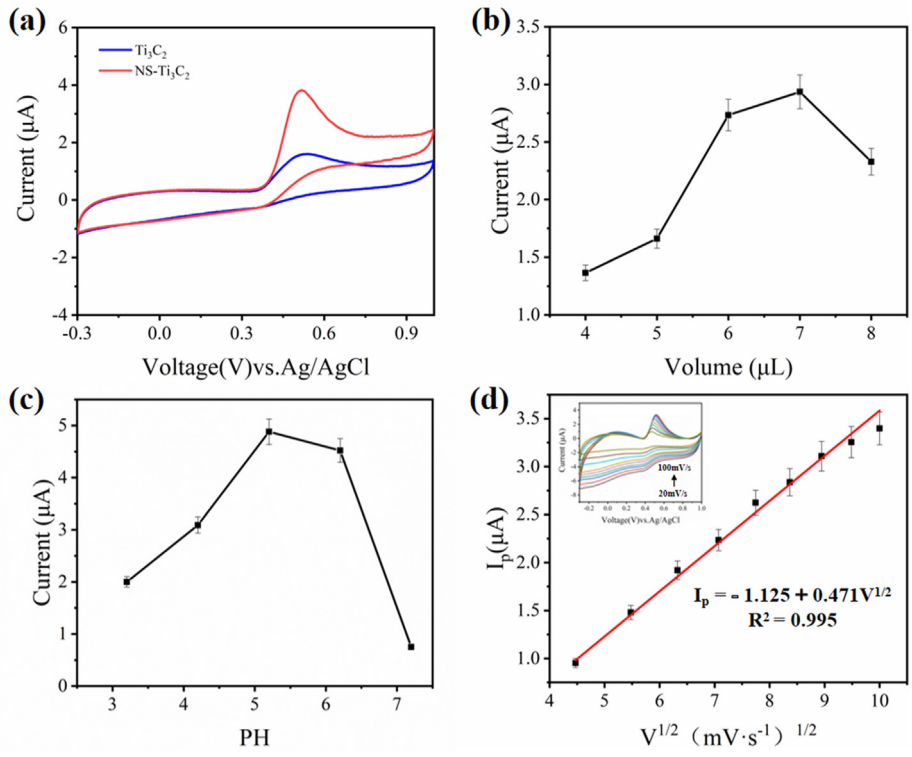

Fig. 6. (a) CV of 100 μM UA at Ti_3C_2 NSs/GCE and NS-Ti_3C_2/GCE in disodium hydrogen phosphate-citrate buffer (pH = 5.2) with the scan rate of 100 mV s^{-1}. (b) Current of NS-Ti_3C_2/GCE in disodium hydrogen phosphate-citrate buffer with different volume containing 100 μM UA.(c)Current of NS-Ti_3C_2/GCE in disodium hydrogen phosphate-citrate buffer with different pH containing 100 μM UA. (d) Linear relationship between the I_p with the $V^{1/2}$, inset: CV of 100 μM UA on NS-Ti_3C_2 NSs/GCE at different scan rates: 20, 30, 40, 50, 60, 70, 80, 90 and 100 mV s^{-1}.

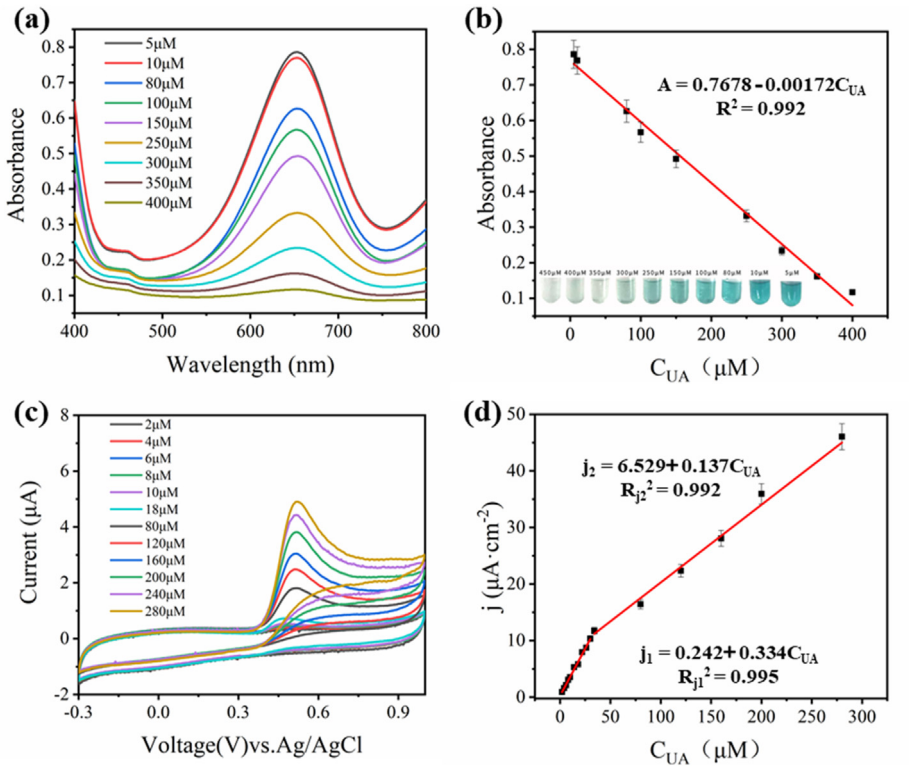

Fig. 7. (a) Absorbance spectra of ox-TMB obtained by varying the concentration of UA from 5 to 400 μM. (b) Nearly linear plot with UA concentrations ranging from 5 to 400 μM, the illustration showed the color change, inset: color change. (c) CV of 2–280 μM UA at NS-Ti_3C_2/GCE in disodium hydrogen phosphate-citrate buffer (pH = 5.2) with the scan rate of 100 mV s^{-1}. (d) Linear relationship between the oxidation peak current density and the concentration of UA. (For interpretation of the references to color in this figure legend, the reader is referred to the Web version of this article.)

study and others. Through comparison, we concluded that the currently proposed UA detection method had a wider detection range and could greatly reduce the pretreatment procedures for samples. In addition, using the colorimetric method, we can easily achieve visual inspection with the naked eye. Relying on the electrochemical analyzer, we can further improve the range and sensitivity of UA detection. These conclusions illustrate the huge application potential of the colorimetric and electrochemical coupling technology in the field of UA detection.

3.6. Real sample and anti-interference analysis

When detecting UA in actual samples, the composition of the solution is very complicated, so the anti-interference ability of the sensing platform has attracted much attention. In order to determine the influence of possible interfering substances on UA detection, tyrosine (10 mM), Cu^{2+} (10 mM), K^+ (10 mM), Na^+ (10 mM), glucose (10 mM), urea (10 mM) and uric acid (200 μM), ascorbic acid (200 μM), cysteine (200 μM) was used to study the specificity of colorimetric and electrochemical methods. When the tyrosine, Cu^{2+}, K^+, Na^+, glucose and urea were added into the system, the absorbance at 652 nm did not change obviously (Fig. S6). However, in the presence of uric acid, ascorbic acid and cysteine, the absorbance had decreased and the color of the solution visibly changed from blue to colorless. Due to the unsatisfactory selectivity of the colorimetric sensor for reducing substances, the selectivity using electrochemical methods was further explored. The amperometric responses to these interferents at 0.53 V are shown in Fig. S7. No obvious interference in UA detection was observed at the applied potential, suggesting that the biosensor has satisfactory selectivity for the detection of UA, which made up for the deficiency of colorimetry. Therefore, all the results indicated that the colorimetric and electrochemical coupling technology can be applied for quantifying UA with reliable selectivity.

To test the practicability of these methods, fresh serum samples were used to detect UA. The standard addition method was used to determine the UA content, and four different serums were mixed with different UA concentrations. As shown in Table 1, in the colorimetric detection process, the recovery rate and RSD of UA in serum were 94.26–104.34% and 2.40–3.63%, respectively; the recovery rate and RSD of the electrochemical method in serum were 93.3–107.33% and 2.36–4.12%, respectively, which proved the good reliability in actual detection.

4. Conclusion

In short, a new structure composed of nitrogen and sulfur co-doped on the surface of Ti_3C_2 nanosheets were used as the peroxidase mimic and electrochemical sensors for the detection of UA. It is revealed that NS-Ti_3C_2 NSs show much higher peroxidase-like and electrochemical activity than Ti_3C_2 NSs. The catalytic mechanism of NS-Ti_3C_2 NSs is composed of two important parts: the dissociation and adsorption of H_2O_2 and the protonation of TMB. Nitrogen accelerates the combination of protonated TMB and •OH by enhancing the adsorption of •OH. Sulfur further increases the distance between the material layer and the layer, and increases the contact area between the catalytically active site and the reactive substrate. In addition, more defects on the surface of NS-Ti_3C_2 NSs also improve the efficiency of electron transfer. Finally, a sensitive colorimetric and electrochemical method is proposed to detect UA. With the optimal conditions, outstanding linear relationship of

Table 1
Application with the method to detect serum spiked with varied UA amounts.

Methods	Samples	Added (μM)	Detected (μM)	Recovery (%)	RSD (%)
UV–vis	Serum 1	10	10.21	102.1	3.09
Electrochemistry		10	9.33	93.3	4.12
UV–vis	Serum 2	50	52.17	104.34	2.40
Electrochemistry		50	48.73	97.46	4.10
UV–vis	Serum 3	100	99.17	99.17	3.63
Electrochemistry		100	100.64	100.64	2.43
UV–vis	Serum 4	200	188.53	94.26	2.89
Electrochemistry		200	214.66	107.33	2.36

absorbance and UA dose ranging from 2 to 400 μM are obtained with LOD of 0.19 μM. The established UA biosensor has high sensitivity, stability, reproducibility and selectivity, which held the application prospect for UA detection in real samples. These conclusions illustrate the huge application potential of the colorimetric and electrochemical coupling technology in the field of UA detection.

CRediT authorship contribution statement

Da Chen: Supervision, Project administration. **Shuaibin Shao:** Writing – original draft, Formal analysis. **Wei Zhang:** Investigation. **Jingbo Zhao:** Validation. **Meiling Lian:** Resources, Conceptualization, Writing – review & editing.

Declaration of competing interest

The authors declare that they have no known competing financial interests or personal relationships that could have appeared to influence the work reported in this paper.

Acknowledgements

We gratefully acknowledge the National Natural Science Foundation of China (22004130, 21973111, 61801519), the Research Startup Fund Project of Civil Aviation University of China (2020KYQD07).

Appendix A. Supplementary data

Supplementary data to this article can be found online at https://doi.org/10.1016/j.aca.2022.339520.

References

[1] C. Wang, S. Chen, L. Song, Tuning 2D MXenes by surface controlling and interlayer engineering: methods, properties, and synchrotron radiation characterizations, Adv. Funct. Mater. 30 (47) (2020).
[2] A.S.F. Vladislav Kamysbayev, Huicheng Hu, Rui Xue, Francisco Lagunas, Di Wang, Robert F. Klie, Dmitri V. Talapin, Covalent surface modifications and superconductivity of two-dimensional metal carbide MXenes, Science 369 (6506) (2020) 979–983.
[3] M. Lu, W. Han, H. Li, W. Zhang, B. Zhang, There is plenty of space in the MXene layers: the confinement and fillings, J. Energy Chem. 48 (2020) 344–363.
[4] X. Li, C. Wang, Y. Cao, G. Wang, Functional MXene materials: progress of their applications, Chem. Asian J. 13 (19) (2018) 2742–2757.
[5] Y.H. Wang, Z.X. Zeng, J.Y. Qiao, S.Q. Dong, Q. Liang, S.J. Shao, Ultrasensitive determination of nitrite based on electrochemical platform of AuNPs deposited on PDDA-modified MXene nanosheets, Talanta 221 (2021) 121605.
[6] H. Zhang, Z. Wang, Q. Zhang, F. Wang, Y. Liu, Ti_3C_2 MXenes nanosheets catalyzed highly efficient electrogenerated chemiluminescence biosensor for the detection of exosomes, Biosens. Bioelectron. 124–125 (2019) 184–190.
[7] M. Liu, Y. He, J. Zhou, Y. Ge, J. Zhou, G. Song, A "naked-eye" colorimetric and ratiometric fluorescence probe for uric acid based on Ti_3C_2 MXene quantum dots, Anal. Chim. Acta 1103 (2020) 134–142.
[8] X. Wu, T. Chen, Y. Chen, G. Yang, Modified Ti_3C_2 nanosheets as peroxidase mimetics for use in colorimetric detection and immunoassays, J. Mater. Chem. B 8 (13) (2020) 2650–2659.
[9] Y. Li, Z. Kang, L. Kong, H. Shi, Y. Zhang, M. Cui, D.P. Yang, MXene-Ti_3C_2/CuS nanocomposites: enhanced peroxidase-like activity and sensitive colorimetric cholesterol detection, Mater. Sci. Eng. C 104 (2019) 110000.
[10] M. Li, H. Wang, X. Wang, Q. Lu, H. Li, Y. Zhang, S. Yao, Ti_3C_2/Cu_2O heterostructure based signal-off photoelectrochemical sensor for high sensitivity detection of glucose, Biosens. Bioelectron. 142 (2019) 111535.
[11] D. Cheng, P. Li, X. Zhu, M. Liu, Y. Zhang, Y. Liu, Enzyme-free electrochemical detection of hydrogen peroxide based on the three-dimensional flower-like Cu-based metal organic frameworks and MXene nanosheets, Chin. J. Chem. 39 (8) (2021) 2181–2187.
[12] J. Liu, W. Lu, X. Lu, L. Zhang, H. Dong, Y. Li, Versatile Ti3C2T x MXene for free-radical scavenging, Nano Res. (2021) 1–9.
[13] X. Hu, X. Sun, Q. Song, Y. Zhu, Y. Long, Z. Dong, N,S co-doped hierarchically porous carbon materials for efficient metal-free catalysis, Green Chem. 22 (3) (2020) 742–752.
[14] M.S. Ansari, T.N. Jebakumar Immanuel Edison, Y.R. Lee, Enhanced electrocatalytic and supercapacitive performance using the synergistic effect of defect-rich N/S co-doped hierarchical porous carbon, Sustain. Energy Fuels 4 (11) (2020) 5697–5708.
[15] L. Yu, Z. Fan, Y. Shao, Z. Tian, J. Sun, Z. Liu, Versatile N-doped MXene ink for printed electrochemical energy storage application, Adv. Energy Mater. 9 (34) (2019).
[16] T.A. Le, Q.V. Bui, N.Q. Tran, Y. Cho, Y. Hong, Y. Kawazoe, H. Lee, Synergistic effects of nitrogen doping on MXene for enhancement of hydrogen evolution reaction, ACS Sustain. Chem. Eng. 7 (19) (2019) 16879–16888.
[17] W.W. Tian, J.T. Ren, X.W. Lv, L.J. Gao, Z.Y. Yuan, N. Melamine-Induced, S-Codoped hierarchically porous carbon nanosheets for enhanced electrocatalytic oxygen reduction, ChemistrySelect 5 (11) (2020) 3477–3484.
[18] H. Guo, R. Gao, M. Sun, H. Guo, B. Wang, L. Chen, Cobalt entrapped in N,S-codoped porous carbon: catalysts for transfer hydrogenation with formic acid, ChemSusChem 12 (2) (2019) 487–494.
[19] J. Li, D. Yan, S. Hou, Y. Li, T. Lu, Y. Yao, L. Pan, Improved sodium-ion storage performance of Ti_3C_2Tx MXenes by sulfur doping, J. Mater. Chem. 6 (3) (2018) 1234–1243.
[20] J. Tang, T. Mathis, X. Zhong, X. Xiao, H. Wang, M. Anayee, F. Pan, B. Xu, Y. Gogotsi, Optimizing ion pathway in titanium carbide MXene for practical high-rate supercapacitor, Adv. Energy Mater. 11 (4) (2020) 2003025.
[21] D. Zhao, Z. Chen, W. Yang, S. Liu, X. Zhang, Y. Yu, W.C. Cheong, L. Zheng, F. Ren, G. Ying, X. Cao, D. Wang, Q. Peng, G. Wang, C. Chen, MXene (Ti_3C_2) vacancy-confined single-atom catalyst for efficient functionalization of CO_2, J. Am. Chem. Soc. 141 (9) (2019) 4086–4093.
[22] Y. Zhang, J. Li, Z. Gong, J. Xie, T. Lu, L. Pan, Nitrogen and sulfur co-doped vanadium carbide MXene for highly reversible lithium-ion storage, J. Colloid Interface Sci. 587 (2021) 489–498.
[23] Q. Li, B. Zhong, W. Zhang, Z. Jia, D. Jia, S. Qin, J. Wang, J.M. Razal, X. Wang, Ti_3C_2 MXene as a new nanofiller for robust and conductive elastomer composites, Nanoscale 11 (31) (2019) 14712–14719.
[24] J. Xia, S.-Z. Yang, B. Wang, P. Wu, I. Popovs, H. Li, S. Irle, S. Dai, H. Zhu, Boosting electrosynthesis of ammonia on surface-engineered MXene Ti_3C_2, Nano Energy (2020) 72.
[25] Y. Li, Q. Liu, S. Zhang, G. Li, The vital balance of graphitization and defect engineering for efficient bifunctional oxygen electrocatalyst based on N-doping carbon/CNT frameworks, ChemCatChem 11 (2) (2019) 861–867.
[26] Z. Ma, X. Xiang, C. Tian, J. Wu, P. Li, B. Li, X. Zu, S. Li, One-step synthesis of N/S codoped "porous carbon cloth" as a sulfur carrier for lithium–sulfur batteries, Energy Technol. 8 (9) (2020).
[27] W. Fang, P. Dai, H. Hu, T. Jiang, H. Dong, M. Wu, Fe0.96S/Co8FeS8 nanoparticles co-embedded in porous N, S codoped carbon with enhanced bifunctional electrocatalystic activities for all-solid-state Zn-air batteries, Appl. Surf. Sci. (2020) 505.
[28] J. Zhou, L. Hou, J. Lian, W. Cheng, D. Wang, H. Gou, F. Gao, Nitrogen-doped highly dense but porous carbon microspheres with ultrahigh volumetric capacitance and rate capability for supercapacitors, J. Mater. Chem. 7 (2) (2019) 476–485.
[29] H. Guo, R. Gao, M. Sun, H. Guo, B. Wang, L. Chen, Cobalt entrapped in N,S-codoped porous carbon: catalysts for transfer hydrogenation with formic acid, ChemSusChem 12 (2) (2019) 487–494.
[30] H. Liu, Z. Hu, Q. Liu, P. Sun, Y. Wang, S. Chou, Z. Hu, Z. Zhang, Single-atom Ru anchored in nitrogen-doped MXene (Ti_3C_2Tx) as an efficient catalyst for the

hydrogen evolution reaction at all pH values, J. Mater. Chem. 8 (46) (2020) 24710–24717.
[31] M.S. Ansari, T.N. Jebakumar Immanuel Edison, Y.R. Lee, Enhanced electrocatalytic and supercapacitive performance using the synergistic effect of defect-rich N/S co-doped hierarchical porous carbon, Sustain. Energy Fuels 4 (11) (2020) 5697–5708.
[32] H. Li, Y. Wen, X. Zhu, J. Wang, L. Zhang, B. Sun, Novel heterostructure of a MXene@NiFe-LDH nanohybrid with superior peroxidase-like activity for sensitive colorimetric detection of glutathione, ACS Sustain. Chem. Eng. 8 (1) (2019) 520–526.
[33] T. Lin, L. Zhong, L. Guo, F. Fu, G. Chen, Seeing diabetes: visual detection of glucose based on the intrinsic peroxidase-like activity of MoS2 nanosheets, Nanoscale 6 (20) (2014) 11856–11862.
[34] L. Hu, Y. Yuan, L. Zhang, J. Zhao, S. Majeed, G. Xu, Copper nanoclusters as peroxidase mimetics and their applications to H_2O_2 and glucose detection, Anal. Chim. Acta 762 (2013) 83–86.
[35] L. Sun, Y. Ding, Y. Jiang, Q. Liu, Montmorillonite-loaded ceria nanocomposites with superior peroxidase-like activity for rapid colorimetric detection of H_2O_2, Sens. Actuators, B 239 (2017) 848–856.
[36] N.V.B. Bhakti R Petigara, Alice C. Mignerey, Mechanisms of hydrogen peroxide decomposition in soils, Environ. Sci. Technol. 36 (2002) 639–645.
[37] O. Adeniyi, S. Sicwetsha, P. Mashazi, Nanomagnet-silica nanoparticles decorated with Au@Pd for enhanced peroxidase-like activity and colorimetric glucose sensing, ACS Appl. Mater. Interfaces 12 (2) (2020) 1973–1987.
[38] F. Cao, L. Zhang, Y. You, L. Zheng, J. Ren, X. Qu, An enzyme-mimicking single-atom catalyst as an efficient multiple reactive oxygen and nitrogen species scavenger for sepsis management, Angew. Chem., Int. Ed. Engl. 59 (13) (2020) 5108–5115.
[39] M. Zhang, Q. Yao, W. Guan, C. Lu, J.-M. Lin, Layered double hydroxide-supported carbon dots as an efficient heterogeneous Fenton-Like catalyst for generation of hydroxyl radicals, J. Phys. Chem. C 118 (2014) 10441–10447.
[40] X. Shen, Z. Wang, X. Gao, Y. Zhao, Density functional theory-based method to predict the activities of nanomaterials as peroxidase mimics, ACS Catal. 10 (21) (2020) 12657–12665.
[41] X. Feng, Z. Yu, R. Long, X. Li, L. Shao, H. Zeng, G. Zeng, Y. Zuo, Self-assembling 2D/2D (MXene/LDH) materials achieve ultra-high adsorption of heavy metals Ni_{2+} through terminal group modification, Separ. Purif. Technol. (2020) 253.
[42] T. Tsuneda, T. Taketsugu, Theoretical investigations on hydrogen peroxide decomposition in aquo, Phys. Chem. Chem. Phys. 20 (38) (2018) 24992–24999.
[43] G. Liu, J. Zou, Q. Tang, X. Yang, Y. Zhang, Q. Zhang, W. Huang, P. Chen, J. Shao, X. Dong, Surface modified Ti3C2 MXene nanosheets for tumor targeting photothermal/photodynamic/chemo synergistic therapy, ACS Appl. Mater. Interfaces 9 (46) (2017) 40077–40086.
[44] W.W. Tian, J.T. Ren, X.W. Lv, L.J. Gao, Z.Y. Yuan, N. Melamine-Induced, S-Codoped hierarchically porous carbon nanosheets for enhanced electrocatalytic oxygen reduction, ChemistrySelect 5 (11) (2020) 3477–3484.
[45] W. Qin, L. Su, C. Yang, Y. Ma, H. Zhang, X. Chen, Colorimetric detection of sulfite in foods by a TMB-O_2-Co_3O_4 nanoparticles detection system, J. Agric. Food Chem. 62 (25) (2014) 5827–5834.
[46] M. Lian, M. Liu, X. Zhang, et al., Template-regulated bimetallic sulfide nanozymes with high specificity and activity for visual colorimetric detection of cellular H_2O_2, ACS Appl. Mater. Interfaces 13 (2021) 53599–53609.
[47] Z.H. Sheng, X.Q. Zheng, J.Y. Xu, W.J. Bao, F.B. Wang, X.H. Xia, Electrochemical sensor based on nitrogen doped graphene: simultaneous determination of ascorbic acid, dopamine and uric acid, Biosens. Bioelectron. 34 (1) (2012) 125–131.
[48] S. Sakthinathan, S. Kubendhiran, S.M. Chen, K. Manibalan, M. Govindasamy, P. Tamizhdurai, S.T. Huang, Reduced graphene oxide non-covalent functionalized with zinc tetra phenyl porphyrin nanocomposite for electrochemical detection of dopamine in human serum and rat brain samples, Electroanalysis 28 (2016) 2126–2135.
[49] C. Ruggiero, A. Cherubini, A. Ble, A.J. Bos, M. Maggio, V.D. Dixit, F. Lauretani, S. Bandinelli, U. Senin, L. Ferrucci, Uric acid and inflammatory markers, Eur. Heart J. 27 (10) (2006) 1174–1181.
[50] D. Liang, T. Yong, S. Chen, Y. Xie, D. Chen, X. Zhou, D. Li, M. Li, L. Su, D. Zuo, Hypouricemic effect of 2,5-dihydroxyacetophenone, a computational screened bioactive compound from ganoderma applanatum, on hyperuricemic mice, Int. J. Mol. Sci. 19 (5) (2018).
[51] K. Arora, M. Tomar, V. Gupta, Highly sensitive and selective uric acid biosensor based on RF sputtered NiO thin film, Biosens. Bioelectron. 30 (1) (2011) 333–336.
[52] M. Sellmayr, M.R. Hernandez Petzsche, Q. Ma, N. Kruger, H. Liapis, A. Brink, B. Lenz, M.L. Angelotti, V. Gnemmi, C. Kuppe, H. Kim, E.M.J. Bindels, F. Tajti, J. Saez-Rodriguez, M. Lech, R. Kramann, P. Romagnani, H.J. Anders, S. Steiger, Only hyperuricemia with crystalluria, but not asymptomatic hyperuricemia, drives progression of chronic kidney disease, J. Am. Soc. Nephrol. 31 (12) (2020) 2773–2792.
[53] D. Cao, Y.X. Luo, W.P. Liu, Y.S. Li, X.F. Gao, Enzyme-free fluorescence determination of uric acid and trace Hg(II) in serum using Si/N doped carbon dots, Spectrochim. Acta Mol. Biomol. Spectrosc. 263 (2021) 120182.
[54] H. Wang, T. Wu, M. Li, Y. Tao, Recent advances in nanomaterials for colorimetric cancer detection, J. Mater. Chem. B 9 (4) (2021) 921–938.
[55] J. Zheng, M. Zhu, J. Kong, Z. Li, J. Jiang, Y. Xi, F. Li, Microfluidic paper-based analytical device by using Pt nanoparticles as highly active peroxidase mimic for simultaneous detection of glucose and uric acid with use of a smartphone, Talanta 237 (2022) 122954.
[56] F. Mazzara, B. Patella, G. Aiello, A. O'Riordan, C. Torino, A. Vilasi, R. Inguanta, Electrochemical detection of uric acid and ascorbic acid using r-GO/NPs based sensors, Electrochim. Acta (2021) 388.
[57] S. Wu, H. Wang, B. Zhao, T. Cao, J. Ma, L. Liu, Z. Tong, Construction of cationic polyfluorinated azobenzene/reduced graphene oxide for simultaneous determination of dopamine, uric acid and ascorbic acid, Talanta 237 (2022) 122986.